Journal of Power Sources 192 (2009) 724–729

Contents lists available at ScienceDirect

Journal of Power Sources

journal homepage: www.elsevier.com/locate/jpowsour

Microstructure and electrochemical corrosion behavior of a Pb–1 wt%Sn alloy for lead-acid battery components

Leandro C. Peixoto, Wislei R. Osório, Amauri Garcia*

Department of Materials Engineering, University of Campinas – UNICAMP, PO Box 612, 13083-970, Campinas - SP, Brazil

ARTICLE INFO

Article history:
Received 12 January 2009
Received in revised form 25 February 2009
Accepted 25 February 2009
Available online 13 March 2009

Keywords:
Pb–Sn alloys
Lead-acid battery grids
Cellular microstructure
Electrochemical corrosion resistance

ABSTRACT

The aim of this study was to evaluate the effect of solidification cooling rates on the as-cast microstructural morphologies of a Pb–1 wt%Sn alloy, and to correlate the resulting microstructure with the corresponding electrochemical corrosion resistance in a 0.5 M H_2SO_4 solution at 25 °C. Cylindrical low-carbon steel and insulating molds were employed permitting the two extremes of a significant range of solidification cooling rates to be experimentally examined. Electrochemical impedance spectroscopy (EIS) diagrams, potentiodynamic polarization curves and an equivalent circuit analysis were used to evaluate the electrochemical corrosion response of Pb–1 wt%Sn alloy samples. It was found that lower cooling rates are associated with coarse cellular arrays which result in better corrosion resistance than fine cells which are related to high cooling rates. The experimental results have shown that that the pre-programming of microstructure cell size of Pb–Sn alloys can be used as an alternative way to produce as-cast components of lead-acid batteries with higher corrosion resistance.

1. Introduction

During the past 20 years, lead-acid batteries manufacturers have focused on modifications of grid manufacturing processes and on the chemical composition of the used alloys in order to decrease battery grid weight as well as to reduce the production costs, and to increase the battery life-time cycle and the corrosion resistance [1–8].

Pb–Sn, Pb–Sb and Pb–Ca–Sn alloys are commonly used in the production of positive and negative grids, connectors, posts and straps components of both VRLA—valve-regulated lead acid and SLI—starting, lighting and ignition batteries in the automotive industry and telecommunication services [1–3]. These components are generally produced by continuous processes such as conventional continuous casting, continuous casting followed by expansion, continuous casting followed by rolling, etc. [1,2]. Prengaman [1] reported that battery components manufactured with Pb–Sb alloys corrode more rapidly than those produced with Pb–Sn and Pb–Sn(Ca) alloys. He states that antimony, e.g. at SLI battery positive grids, enhances electrolysis of water into hydrogen and oxygen during charging, leading to water or electrolyte loss. On the other hand, the use of Pb–Sn and Pb–Sn(Ca) alloys can be an effective way to minimize gassing, water and electrolytic solution losses. Due to this, these alloys can be better alternatives for the production of Pb-acid battery grids with a view to achieve a maintenance-free condition [1–13].

The selection of appropriate alloy compositions for battery grids involves considerations of grid-production capability, economic feasibility, and metallurgical and electrochemical properties of the resulting alloys. The most effective method way to manufacture highly resistant Pb alloys battery grids is to reduce all impurities and alloying elements as much as possible, i.e., to keep the grid composition as close as possible to pure lead. The effects of alloying additions to Pb-based alloys have been studied for a wide range of alloy compositions. Calcium additions in the range of 0.02–0.05 wt% are usually made in order to improve the resulting mechanical properties. However, due to its segregation to the grain boundaries and interdendritic regions it can considerably affect the corresponding corrosion resistance in the pasting/curing process. The grid must be corroded along this process to permit the paste to adhere to the grid. The addition of Sn in the range between 0.3 and 1.5 wt% is commonly used [2,10], despite its complex role on the kinetics of formation, passivation and growth of PbO and PbO_2 layers [14]. For Pb–Sn–Ca alloys the Sn content must be sufficient to react with all the calcium in the alloy to produce Sn_3Ca, a more stable strengthening precipitate instead of Pb_3Ca. Lead–calcium alloy grids have also been improved by the addition of silver in the range of 0.02–0.05 wt%. These alloys have higher mechanical properties and creep resistance and greater dimensional stability [1].

The cellular and dendritic spacings are important microstructural parameters affecting the microscopic segregation between these morphologic ramifications and the mechanical properties.

* Corresponding author. Tel.: +55 19 3521 3320; fax: +55 19 3289 3722.
E-mail address: amaurig@fem.unicamp.br (A. Garcia).

0378-7753/$ – see front matter © 2009 Elsevier B.V. All rights reserved.
doi:10.1016/j.jpowsour.2009.02.081

The resulting microstructure array spacing was also shown to strongly influence the overall surface corrosion resistance of binary alloys [14–18].

It is known that low growth rates during solidification and/or low alloy solute content can favor the growth of regular cells. On the other hand, dendritic microstructures are typical of alloys with higher solute content and/or solidified under high growth rates. Both the macro- and microstructural arrays affect the mechanical properties and the corrosion resistance [16–18]. It was found that the improvement on the corrosion resistance depends on the cooling rate imposed during solidification which affects dendrite arm size and solute redistribution, and on the electrochemical behavior of solute and solvent [16–18]. In a recent experimental study with Pb–Sb [19] alloys subjected to corrosion tests in a 0.5 M H_2SO_4 solution, it was shown that coarse cellular samples were associated with better electrochemical corrosion resistance than fine cellular samples.

Rezaei and Damiri [7] have also stated that the control of solidification variables has an important role on the electrochemical behavior of lead-acid battery grid alloys. These authors reported that lower cooling rates imposed during solidification of a lead-antimony alloy casting provided antimony segregation to the interior of the casting, while surface antimony concentration had significantly decreased.

Considering the diversity of commercially battery-component manufacturing processes, a homogeneous composition of the grid or strap battery component can represent a great challenge when three or more elements are added. The lead-acid battery manufacturers should alternatively consider the pre-programming of the resulting microstructure of binary alloys by controlling solidification variables as an important tool for the improvement of the resulting mechanical properties and corrosion response. This study correlates and corrosion behavior of an as-cast Pb–1 wt%Sn alloy in a 0.5 M H_2SO_4 solution at 25 °C. The effect of very different cooling rates, typical of casting processes which use metallic molds and insulating molds, on the morphology and scale of the microstructural pattern was examined.

2. Experimental procedure

Experiments were carried out with a Pb–1 wt%Sn alloy which was prepared by using 99.89 and 99.99 wt% pure Pb and Sn, respectively. The main impurities were Fe (0.10%), Si (0.07%), Cu (0.02%), besides other minor elements with concentration less than 50 ppm.

A low-carbon steel (SAE 1020) mold with an internal diameter of 50 mm, height 50 mm and a 3 mm wall thickness was used. Initially, the Pb–1%Sn alloy was melted in an electric resistance-type furnace until the molten Pb–Sn alloy reached a temperature of ±340 °C (of about 10% above the liquidus temperature). It was then stirred, degassed and poured into the casting chamber (low-carbon steel mold). Two experiments were carried out for different mold conditions before pouring: (i) mold surface polished and kept at the room temperature (±25 °C) and (ii) mold surface completely covered with an insulating alumina layer (of about 1 mm thick) to minimize heat losses and with the mold pre-heated at 200 °C (±5 °C). The former condition has permitted higher cooling rates to be attained during solidification (in a range from 8 to 12 K s^{-1}) and the latter condition has induced lower cooling rates (from 0.5 to 1 K s^{-1}). Temperatures were monitored via type J thermocouples.

As-cast specimens were sectioned from the center of the ingot, ground, polished and etched to reveal the macrostructure (the etchant was a mixture of aqueous solutions: 3:1 – in volume – HNO_3 solution and 6:1 – in volume – ammonium molybdate). The samples were polished and etched by using a 37 cm^3 glacial acetic acid and 15 cm^3 of hydrogen peroxide solution at room temperature for microscopy examination. The microstructural characterization was carried out by using an optical microscope associated with an image processing system Neophot 32 (Carl Zeiss, Esslingen, Germany) and Leica Quantimet 500 MC (Leica Imaging Systems Ltd., Cambridge, England) [19,20].

In order to evaluate the electrochemical corrosion behavior of the Pb–1%Sn alloy samples, electrochemical corrosion tests were performed in a 1 cm^2 circular area of ground (600 grit SiC finish) sample surfaces. Electrochemical impedance spectroscopy (EIS) measurements began after an initial delay of 30 min for the samples to reach a steady-state condition. The tests were carried out with the samples immersed in a stagnant and naturally aerated 500 cm^3 of a 0.5 M H_2SO_4 solution at 25 °C under a pH of about 0.88, used to simulate the battery electrolytic fluid. A potentiostat (EG & G Princeton Applied Research, model 273A) coupled to a frequency analyzer system (Solartron model 1250), a glass corrosion cell kit with a platinum counter-electrode and a saturated calomel reference electrode (SCE) were used to perform the EIS tests. The potential amplitude was set to 10 mV, peak-to-peak (AC signal), with 5 points per decade and the frequency range was set from 100 mHz to 100 kHz at open circuit. The samples were further ground to a 1200 grit SiC finish, followed by distilled water washing and air drying before measurements.

Potentiodynamic measurements were also carried out in the aforementioned solution at 25 °C using a potentiostat at the same positions where the EIS tests were carried out. These tests were performed by stepping the potential at a scan rate of 0.2 mV s^{-1} from −0.800 mV (SCE) to +2800 mV (SCE), i.e.: −1.24 V to +2.36 V *vs.* MSE. Using an automatic data acquisition system, the potentiodynamic polarization curves were plotted and both corrosion rate and potential were estimated by Tafel plots using both anodic and cathodic branches at a scan rate of 0.2 mV s^{-1} from −250 mV (SCE) to +250 mV (SCE). This mentioned potentiodynamic range corresponds to −1200 mV and −700 mV *vs.* Hg/Hg_2SO_4 electrode (MSE). Although the SCE electrode is not commonly used in lead-acid system studies, a SCE electrode can also be used as a reference electrode since the one inconvenient is the fact that chloride may contaminate the electrolyte, and other is to convert from SCE to MSE or other potential scales (ASTM G3).

Duplicate tests for EIS and potentiodynamic polarization curves were carried out. In order to supply quantitative support for discussions of these experimental EIS results, an appropriate model (ZView version 2.1b) for equivalent circuit quantification was used.

3. Results and discussion

3.1. Resulting as-cast structures

Fig. 1 shows the resultant multidirectional casting macrostructures (randomly oriented grains). It can be seen that the growth of both fine and coarse equiaxed grains have prevailed along the entire casting. The average grain sizes of fine and coarse equiaxed Pb–1%Sn alloy castings are 2 mm and 7 mm, respectively. These average grain sizes are associated to cooling rates from 8 to 12 K s^{-1} (mold with a polished inner surface) and from 0.5 to 1 K s^{-1} (mold surface covered by an alumina layer), respectively.

Typical microstructures observed along the cross sections of the Pb–1 wt%Sn alloy castings are shown in Fig. 2. The as-cast microstructure consists of a completely cellular array, constituted by a Pb-rich matrix (α-phase: solid solution of Sn in Pb) with a eutectic mixture in the intercellular regions. The cellular spacing for regions solidified under low cooling rates was about 180 μm (±15 μm) with the Pb-rich cellular matrix represented by dark regions with the eutectic mixture being represented by light regions. On the other hand, under higher cooling rates during solidification the resulting cellular spacing was 30 μm (±2.5), i.e., about six times smaller than that of the coarse cells. The coarse and

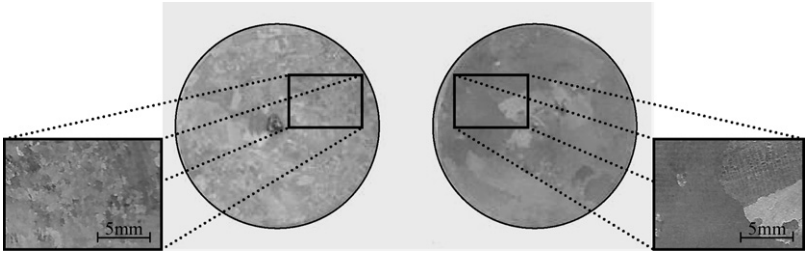

Fig. 1. Typical multidirectional casting macrostructures of Pb–1 wt%Sn alloy with: (a) fine and (b) coarse equiaxed grains obtained solidified under cooling rates from 8 to 12 K s^{-1} (mold with a polished inner surface) and from 0.5 to 1 K s^{-1} (mold surface covered by an alumina layer), respectively.

fine cellular structures had as consequence an experimental average number of cells per surface area of about 45 cells mm^{-2} and 1680 cells mm^{-2}, respectively.

3.2. Electrochemical behavior measurements and equivalent circuit analysis

Although accelerated corrosion testing has been widely used since the early 1900s [21], for some particular situations, excessive aggressiveness of the test solution could mask the real materials performance [21–24]. A number of researchers [16–34] have employed electrochemical impedance spectroscopy techniques to study the corrosion phenomenon. It was reported that these techniques involve some difficulties, one of which is that the equivalent circuit model can be designed in more than one way, so that the impedance spectrum is difficult to be analyzed [25]. In the present investigation, both a polarization method and a qualitative electrochemical technique were chosen to provide a consistent and useful way to investigate the tendency of the corrosion resistance.

Fig. 3 depicts the Bode and Bode-phase diagrams representing the modulus of impedance and phase angle as a function of frequency. The Bode-phase results indicate that two time constants can be associated to the kinetics of corrosion of coarse and fine cellular arrays of the Pb–1%Sn alloy. At a frequency range from 10^3 to 10^5 Hz, the first time constant which can be related with the reaction between the electrolyte and the tin-rich phase in the intercellular region is clearly observed. At low frequencies, in a range of about 0.1 and 50 Hz, the second time constant appears and can be correlated to the reaction with the Pb-rich matrix.

At a frequency of 0.1 Hz, the coarse and fine cellular arrays have presented moduli of impedance of about 3 kΩ cm^{-2} and 1.5 kΩ cm^{-2}, respectively. Considering the Bode-phase diagrams, maximum phase angles ($\theta_{máx.}$) of about 66° in a frequency of 19 Hz and 56° in 38 Hz are observed for coarse and fine cellular spacings, respectively. These experimental impedance parameters give clear

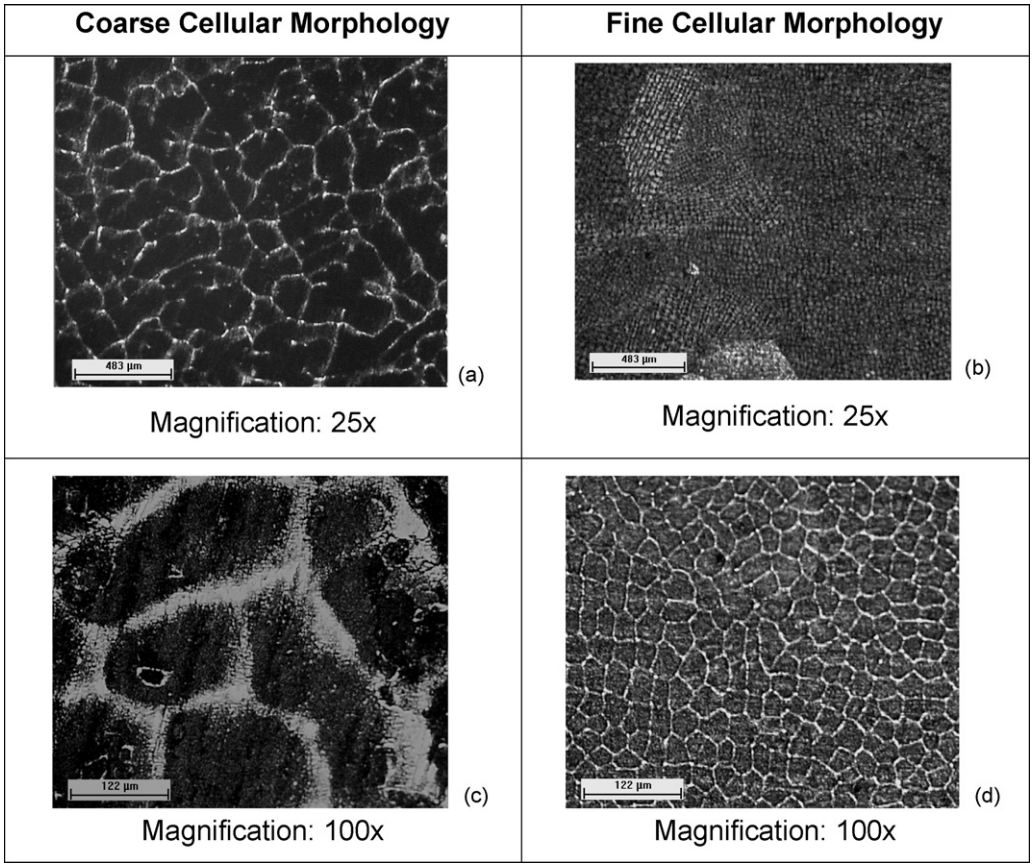

Fig. 2. Typical cellular morphologies along the cross sections of the Pb–1 wt%Sn alloy castings: (a and c) obtained with cooling rate from 0.5 to 1 K s^{-1}; cell spacing λ_c = 180 μm (±15 μm) and (b and d) from 8 to 12 K s^{-1}; λ_c = 30 μm (±2.5 μm).

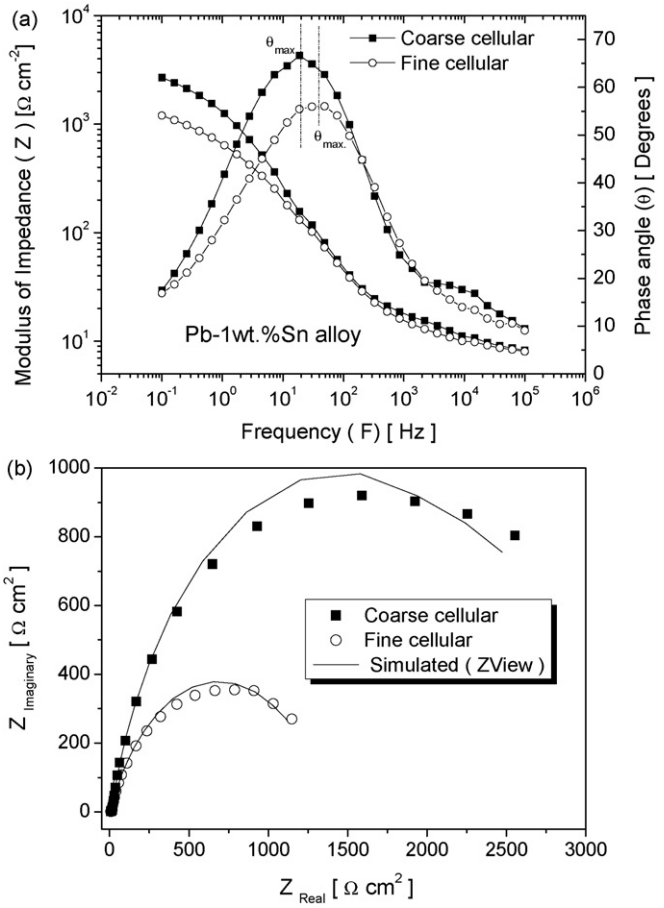

Fig. 3. (a) Experimental EIS diagrams (*Bode and Bode-phase*); (b) experimental and simulated Nyquist results for coarse and fine cellular morphologies of the Pb–1 wt%Sn alloy in a 0.5 M H_2SO_4 solution at room temperature.

indication that the coarse cellular array of the Pb–1%Sn alloy can be related to better electrochemical behavior when compared to the results which correspond to the fine cellular array.

An equivalent circuit analysis has also been conducted, which is similar to those developed in previous articles [25–34]. The proposed equivalent circuit used to fit the experimental data is shown in Fig. 4. The impedance parameters obtained by the ZView® software, are shown in Table 1. The fitting quality was evaluated by chi-squared (χ^2) values of about 20×10^{-4} [19,20,26–34], as shown in Table 1.

In the equivalent circuit, R_{el} denotes the electrolyte resistance which in Bode plot is expressed in a high frequency limit ($F > 1$ kHz), R_1 is the charge transfer resistance, and R_2 ($F < 0.1$ Hz) stands for a polarization resistance due to the participation of adsorbed intermediates. $Z_{CPE(1)}$ and $Z_{CPE(2)}$ denote the double layer capacitance and the capacitance associated with the polarization resistance R_2. The parameters n_1 and n_2 are correlated with the phase angle, varying between −1 and 1. A constant-phase element representing a shift from an ideal capacitor was used instead of the capacitance itself, for simplicity. The impedance of a phase element is defined as $Z_{CPE} = [C(j\omega)^n]^{-1}$ [19,20,26–34], where C is the capacitance; j is the electric current; ω is the frequency and $-1 \leq n \leq 1$. The value of n seems to be also associated with the non-uniform distribution of current as a result of surface roughness and defects [19,20,26–34].

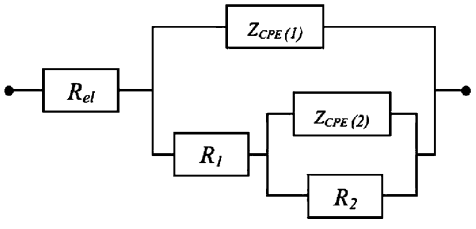

Fig. 4. Proposed equivalent circuit used to obtain impedance parameters.

Table 1
Impedance parameters obtained by the ZView® software by fitting experimental and simulated results for Pb–1 wt% Sn alloy samples in a 0.5 M H_2SO_4 solution at room temperature.

Parameters	Coarse cellular morphology	Fine cellular morphology
R_{el} ($\Omega\,cm^{-2}$)	7.32	6.84
$Z_{CPE(1)}$ ($\mu F\,cm^{-2}$)	120 (±12)	302 (±21)
$Z_{CPE(2)}$ ($\mu F\,cm^{-2}$)	39.20 (±0.5)	33.62 (±2.5)
n_1	0.65	0.58
n_2	0.93	0.91
R_1 ($\Omega\,cm^{-2}$)	16.5	12.5
R_2 ($\Omega\,cm^{-2}$)	3019	1405
χ^2	23×10^{-4}	20×10^{-4}

Simulated and experimental results in Nyquist diagrams for the coarse and fine cellular arrays of the Pb–1%Sn alloy in sulfuric acid solution are shown in Fig. 3(b). Nyquist plots reveal that the diameter of the capacitive arc for coarse cellular spacings is higher than that for fine cellular spacings. These results point to a similar corrosion tendency when compared to those analyzed in Bode and Bode-phase plots, shown in Fig. 3(a).

In Table 1, it can be observed that $Z_{CPE(1)}$ and $Z_{CPE(2)}$ for fine cellular spacings are higher than the corresponding values for coarse spacings. These capacitances are also associated with lowest resistances R_1 and R_2, which indicate that the coarse cellular array has better electrochemical corrosion resistance than the fine cellular structure.

Fig. 5(a) shows partial potentiodynamic polarization curves (from −0.75 V to −0.30 V *vs.* SCE) for coarse and fine cellular Pb–1%Sn alloy samples. The corrosion current density (i_{corr}) was obtained from Tafel plots using both the cathodic and anodic branches of the polarization curves. Such results reinforce the previous corrosion resistance tendency observed with the results of EIS and impedance parameters (equivalent circuit).

In the sweep ranges, shown in Fig. 5(a) and (b), various processes take place and different electrode systems are formed. As a result, different types of EIS equivalent circuits are required, and changes in the component values are necessary. On the other hand, considering the qualitative analysis which was developed using the Bode, Bode-phase and Nyquist diagrams, the selected equivalent circuit (Fig. 4) has been proposed. The constant times, the fitting quality (chi-squared values) and the wide application of this equivalent circuit were also reasons to select this circuit. Considering a same equivalent circuit is possible to compare the effect of different metallographic structures on the resulting general corrosion responses.

Although the fine cellular array has a corrosion potential slightly displaced toward the less noble-side (of about 20 mV *vs.* SCE) when compared to that of the coarse morphology, its correspondent corrosion current density (±37 $\mu A\,cm^{-2}$) is of about six (6) times higher than that corresponding to the coarse cellular array (±6 $\mu A\,cm^{-2}$). The present experimental results have shown that coarser cells tend to improve the corrosion resistance. Grain and cellular boundaries are regions with higher level of energy due to distortions and deformation caused by growth during solidification being more susceptible to the corrosion action. Coarser cells exhibit fewer boundaries providing a better galvanic protection when compared to a fine cellular array, which will be subjected to a more

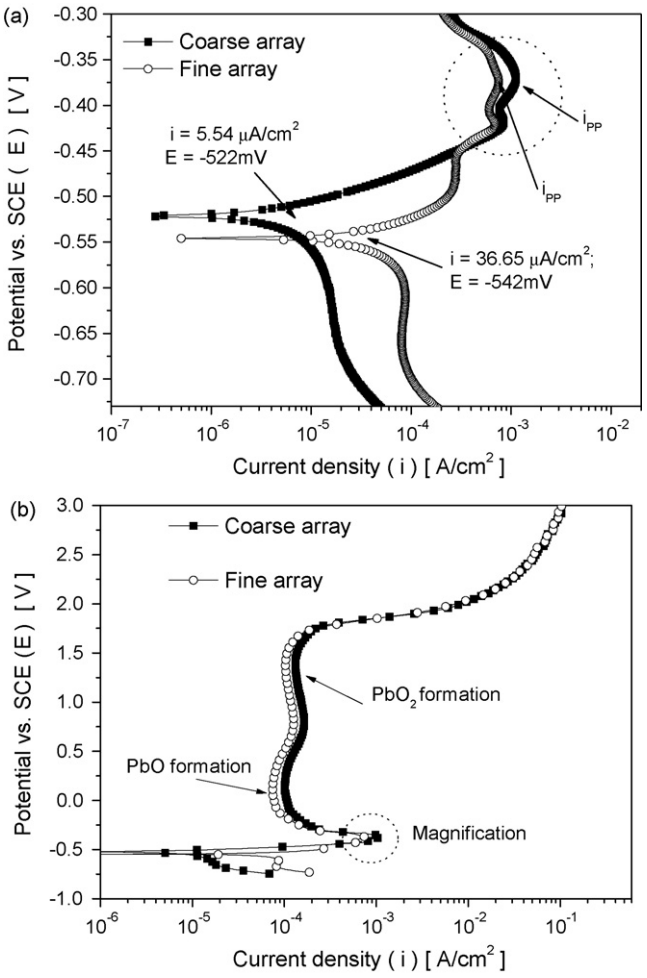

Fig. 5. (a) Experimental potentiodynamic polarization curves exhibiting current densities and corrosion potentials for coarse and fine cellular morphologies and (b) experimental anodic potentiodynamic polarization curves: Pb–1 wt%Sn alloy samples in a 0.5 M H_2SO_4 solution at 25 °C.

extensive corrosion action. In this context it can be said that corrosion in dilute Pb–Sn alloys is similar to that observed in pure metals with equiaxed grains [12,13,16,17]. It is also important to remark that owing to segregation during the cellular growth, the intercellular regions at the cells boundaries will have the highest tin content (one of the phases of the eutectic mixture). By analyzing a galvanic series table [35], it can be seen that tin (Sn) has a potential between −0.30 V and −0.33 V (*vs.* SCE) and lead (Pb) of about −0.19 V to −0.25 V (*vs.* SCE), which indicates that Sn is less noble than Pb.

Fig. 5(b) shows the experimental anodic potentiodynamic polarization curves for both coarse and fine cellular Pb–1%Sn alloy samples in a 0.5 M H_2SO_4 solution at room temperature. A partial stabilization on current density is observed at about 3×10^{-4} A cm^{-2} at a potential of −0.44 V (*vs.* SCE) or −0.81 V (*vs.* MSE) for both potentials of coarse and fine Pb–1%Sn alloy samples, which indicates precipitation and dissolution mechanism of $PbSO_4$ particles. It is important to remark that the solubility of $PbSO_4$ in 0.5 M H_2SO_4 is relatively high and only small amounts of $PbSO_4$ crystals will be formed and reduced (dissolution–precipitation mechanism). According to Pavlov et al. [36–38], it is suggested that the open circuit potential of Pb–1%Sn alloys is something lower than pure lead (−0.95 V *vs.* MSE or −0.58 V *vs.* SCE) due to the accelerated self-discharge related to lower hydrogen overvoltage on the Sn electrode. At potentials above −0.95 V (MSE) which correspond to a range of about −580 mV to −540 mV *vs.* SCE in Fig. 5(b), anodic oxidation of Pb takes place and Pb (II) ions are formed. Some $PbSO_4$ crystals are formed on the electrode surface which, after long enough polarization will form a semi-permeable membrane which, on turn, will passivate the electrode surface. A $PbSO_4$ membrane layer will be formed on the electrode surface (passivation) but not any PbO particle since a high and strong passivation for this formation is demanded [13,36–38].

At a potential of about −0.45 V (*vs.* SCE) corresponding to −0.8 V (*vs.* MSE) the anodic oxidation of Pb to Pb (II) ions begins. Associated with this potential, fine and coarse cellular arrays exhibit current densities of about 7×10^{-4} and 9×10^{-4} A cm^{-2}, respectively. However, it is known that the rate of anodic oxidation of Pb to Pb (II) ions at potentials about −0.8 V (*vs.* MSE) or −0.45 V (*vs.* SCE) is not the process that determines the corrosion rate of lead in sulfuric acid. In addition to the anodic oxidation of lead, at potentials above −0.45 V (*vs.* MSE) or −0.08 V (*vs.* SCE) another anodic process begins in which Sn oxidation to Sn (II) and Sn (IV) can be involved.

Stabilization in the current density for the fine (8×10^{-5} A cm^{-2}) and the coarse (10^{-4} A cm^{-2}) cellular spacings at a same potential of about −0.45 V (*vs.* MSE) or −0.08 V (*vs.* SCE) can be observed in Fig. 5(b), which correspond to PbO formation. In this potential range, selected Pb^{2+} will be formed or reduced along with some hydrogen and/or oxygen evolution. At a potential of about +0.22 V (vs. SCE) or −0.15 V (*vs.* MSE), slight breakdown of potential for both fine and coarse cellular morphologies are observed. Above +1.28 V (*vs.* SCE) or +0.95 V (*vs.* MSE) associated with current densities of 1.0×10^{-4} and 1.3×10^{-4} A cm^{-2}, for the fine and coarse cellular arrays, respectively, PbO_2 is formed. These processes are systematically detailed by Pavlov et al. [36–38].

As aforementioned, the reactions concerning to sulfate precipitation and dissolution, and PbO and PbO_2 formations, occurred firstly for the fine cellular morphology which is also an indication that this morphology is more susceptible to corrosion action than coarse ones.

The present experimental results have shown that the control of as-cast cellular microstructures, by manipulating solidification processing variables can be used as an alternative way to produce as-cast components of lead-acid batteries with higher corrosion resistance. In this context, a high cooling rate casting process will induce a deleterious effect on the general electrochemical corrosion response for dilute Pb–Sn alloys (cellular microstructure) when considering conventional manufacturing of lead-acid battery components.

4. Conclusion

The experimental EIS diagrams, impedance parameters, anodic potentiodynamic polarization curves and the fitted equivalent circuit parameters have shown that coarse cellular structures tend to yield higher corrosion resistance than fine cellular morphologies for an as-cast Pb–1%Sn alloy. Such trend is associated with the reduction of cellular boundaries of coarse cellular arrays when compared with finer cells, since the boundary has proved to be more susceptible to the corrosion action. These results indicate that the control of as-cast cellular microstructures, by manipulating solidification processing variables permitting the control of cooling rate, can be used as an alternative way to produce as-cast components of Pb–Sn dilute alloys for battery components with improved corrosion resistance.

Acknowledgements

The authors acknowledge financial support provided by FAPESP (The Scientific Research Foundation of the State of São Paulo, Brazil), FAEPEX-UNICAMP, and CNPq (The Brazilian Research Council).

References

[1] R.D. Prengaman, J. Power Sources 95 (2001) 224–233.
[2] R.D. Prengaman, J. Power Sources 158 (2006) 1110–1116.
[3] R.D. Prengaman, in: K.R. Bullock, D. Pavlov (Eds.), Proceedings, Advances in Lead-Acid Batteries, vol. 84-14, The Electrochemical Society, Pennington, NJ, 1984, p. 201.
[4] M.D. Achtermann, M.E. Greenlee, J. Power Sources 33 (1991) 87–92.
[5] J. Wirtz, Batteries Int. (January) (1996) 56.
[6] G.S. Al-Ganainy, M.T. Mostafa, F. Abd El-Salam, Physica B 348 (2004) 242–248.
[7] B. Rezaei, S. Damiri, J. Solid State Electrochem. 9 (2005) 590–594.
[8] M. Shiota, T. Kameda, K. Matsui, N. Hirai, T. Tanaka, J. Power Sources 144 (2005) 358–364.
[9] T. Hirasawa, K. Sasaki, M. Taguchi, H. Kaneko, J. Power Sources 85 (2000) 44–48.
[10] C.S. Lakshmi, J.E. Manders, D.M. Rice, J. Power Sources 73 (1998) 23–29.
[11] S. Stein, G. Bourguinon, L. Raboin, L. Broch, L. Johann, E. Rocca, Thin Solid Films 455–456 (2004) 735–741.
[12] W.R. Osório, C.S.C. Aoki, A. Garcia, J. Power Sources 185 (2008) 1471–1477.
[13] W.R. Osório, C.S.C. Aoki, A. Garcia, Mater. Sci. Forum 595–598 (2008) 851–859.
[14] E. Rocca, J. Steinmetz, Electrochim. Acta 44 (1999) 4611–4618.
[15] O.L. Rocha, C.A. Siqueira, A. Garcia, Mater. Sci. Eng. A 361 (2003) 111–118.
[16] W.R. Osório, C.M.A. Freire, A. Garcia, Mater. Sci. Eng. A 402 (2005) 22–32.
[17] W.R. Osório, C.A. Siqueira, C.M.A. Freire, A. Garcia, Rev. Metal. Madrid Extr. (2005) 176–180.
[18] W.R. Osório, P.R. Goulart, G.A. Santos, C. Moura Neto, A. Garcia, Metall. Mater. Trans. 37A (2006) 2525–2537.
[19] W.R. Osório, D.M. Rosa, A. Garcia, J. Power Sources 175 (2008) 595–603.
[20] D.M. Rosa, J.E. Spinelli, W.R. Osório, A. Garcia, J. Power Sources 162 (2006) 696–705.
[21] C.L. Meade, Met. Finish. 98 (2000) 540–542.
[22] A. Conde, J. Damborenea, Corros. Sci. 39 (1997) 295–303.
[23] A. Conde, R. Colaço, R. Vilar, J. Damborenea, Mater. Des. 21 (2000) 441–445.
[24] D. Li, Y. Hu, B. Guo, Mater. Sci. Eng. 280A (2000) 173–176.
[25] F. Mansfeld, M.W. Kendig, J. Electrochem. Soc. 135 (1998) 828–835.
[26] J. Pan, D. Thierry, C. Leygraf, Electrochim. Acta 41 (1996) 1143–1153.
[27] M. Kliskic, J. Radosevic, S. Gudic, M. Smith, Electrochim. Acta 43 (1998) 3241–3255.
[28] M. Aziz-Kerrzo, K.G. Conroy, A.M. Fenelon, S.T. Farell, C.B. Breslin, Biomaterials 22 (2001) 1531–1538.
[29] S. Gudic, J. Radosevic, M. Kliskic, Electrochim. Acta 47 (2002) 3009–3016.
[30] S.L. Assis, S. Wolynec, I. Costa, Electrochim. Acta 51 (2006) 1815–1819.
[31] W.R. Osório, N. Cheung, J.E. Spinelli, P.R. Goulart, A. Garcia, J. Solid State Electrochem. 11 (2007) 1421–1429.
[32] W.R. Osório, P.R. Goulart, A. Garcia, Mater. Lett. 62 (2008) 365–369.
[33] D.Q. Martins, W.R. Osório, M.E.P. Souza, R. Caram, A. Garcia, Electrochim. Acta 53 (2008) 2809–2817.
[34] A. Cremasco, W.R. Osório, C.M.A. Freire, A. Garcia, R. Caram, Electrochim. Acta 53 (2008) 4867–4875.
[35] Australasian Corrosion Association Inc., Galvanic Series: Corrosion Potentials in Flowing Seawater. http://www.corrosion.com.au/documents (accessed August 14, 2008).
[36] D. Pavlov, M. Bojinov, T. Laitinen, G. Sundholm, Electrochim. Acta 36 (1991) 2087–2092.
[37] D. Pavlov, M. Bojinov, T. Laitinen, G. Sundholm, Electrochim. Acta 36 (1991) 2081–2086.
[38] D. Pavlov, B. Monahov, G. Sundholm, T. Laitinen, J. Electroanal. Chem. 305 (1991) 57–63.